Adaptive Harmonic Virtual Impedance Control for Improving Voltage Quality of Microgrids

Yang Wang, Xiang Zhou, Junmiao Tang, Xianyong Xiao, Shu Zhang, and Jiandong Si

***Abstract*—The effects of nonlinear loads on voltage quality represent an emerging concern for islanded microgrids. Existing research works have mainly focused on harmonic power sharing among multiple inverters, which ignores the diversity of different inverters to mitigate harmonics from nonlinear loads. As a result, the voltage quality of microgrids cannot be effectively improved. To address this issue, this study proposes an adaptive harmonic virtual impedance (HVI) control for improving voltage quality of microgrids. Based on the premise that no inverter is overloaded, the main objective of the proposed control is to maximize harmonic power absorption by shaping the lowest output impedances of inverters. To achieve this, the proposed control is utilized to adjust the HVI of each inverter based on its operation conditions. In addition, the evaluation based on Monte Carlo harmonic power flow is designed to assess the performance of the proposed control in practice. Finally, comparative studies and control-in-the-loop experiments are conducted.**

***Index Terms*—Microgrid, nonlinear load, residual capacity, harmonic power, inverter, adaptive harmonic virtual impedance control.**

I. Introduction

MICROGRIDS, which are small power systems that integrate distribution generations (DGs), loads, and energy storage devices, have increased development in recent years [1]. One of their most attractive features is the flexible operation in either grid-connected or islanded modes [2]. In the islanded mode, multiple DGs must properly share the total power demand based on their power ratings [3]. To achieve this, various centralized [4] and decentralized [5] controls have been proposed for interfacing inverters, among which the droop control has received considerable attention because of its plug-and-play feature [6], [7]. Conventional droop control adopts a droop relationship between active power-frequency (P-f) and reactive power-voltage (Q-V) to regulate the voltage and frequency, respectively. Since the voltage magnitude at different locations may not be consistent, as with the frequency, the reactive power sharing is more challenging [8]. Accordingly, several solutions have been proposed [9]-[11], such as adding a secondary control scheme [10] or using virtual impedance control [11].

However, because of the increasing number of nonlinear devices in residential, commercial, and industrial loads, the voltage distortion in a microgrid is a major issue [12]-[14]. To ensure the safe operation of inverters, they must absorb a proper amount of harmonic power. Yet, because of the difference in output impedances, inverters with small capacity may absorb too much power, resulting in an overloaded condition [15]. Therefore, reasonable allocation of harmonic power is important, and most of the latest research works have focused on achieving harmonic sharing, i. e., sharing the harmonic power according to the rated capacity. To achieve this goal, a widely adopted solution involves adding harmonic virtual impedance (HVI) [13]-[16] at the desired frequency. For example, [16] proposes a decentralized control that adjusts the HVI to achieve harmonic power sharing. However, as the HVI is designed to be positive, the decentralized control increases the equivalent impedance of the DG and may worsen the voltage quality.

Regarding the issue of voltage quality, some research works have proposed an advanced HVI control that can simultaneously deal with voltage quality and harmonic sharing. These methods can be divided into centralized [17]-[20] and decentralized [21]-[23] controls. As centralized control typically has high communication demands and computational burdens, only decentralized control is reviewed in this study. Reference [21] proposes a negative HVI control by defining a linear relationship between the HVI value and the inequality between the residual capacity and the harmonic power of the inverter, which guarantees the harmonic sharing performance and improves the power quality to some extent. However, designing this linear relationship is challenging. Based on [21], [22] introduces an additional compensation factor for flexibly adjusting HVI at each harmonic frequency of concern. In [23], the HVI is dynamically adjusted based on the harmonic distortion at the point of common coupling (PCC) with the goal of controlling the voltage distortion within a certain limit, e. g., 5%. Note that harmonic sharing is the primary objective of [21]-[23]. Thus, the performances on voltage quality enhancement are limited.

Based on this background, this study proposes a decentralized adaptive HVI control with the objective of optimizing

Manuscript received: June 30, 2023; revised: September 17, 2023; accepted: November 1, 2023. Date of CrossCheck: November 1, 2023. Date of online publication: November 17, 2023.

This work was supported by the Science and Technology Project of State Grid Corporation of China (No. 5400-202219417A-2-0-ZN).

Y. Wang, X. Zhou, J. Tang, X. Xiao, and S. Zhang (corresponding author) are with the College of Electrical Engineering, Sichuan University, Chengdu 610065, China (e-mail: fwang@scu. edu. cn; 710792368@qq. com; tangjunmiao12@163.com; xiaoxianyong@163. com; ZS20061621@163.com).

J. Si is with the Taizhou Power Supply Company, State Grid Zhejiang Electric Power Co., Ltd., Taizhou 318000, China (e-mail: 2838341399@qq.com).

DOI: 10.35833/MPCE.2023.000447

the voltage quality of the microgrid. The goal of sharing is to guarantee fairness and prevent overloading. When DGs in a microgrid belong to the same owner such as a local utility company, fairness may be less important than the power quality. However, harmonic sharing is not the only way to prevent overloading. Other solutions are available, including real-time monitoring of the absorbed harmonic power within an acceptable limit. Based on the premise that all DGs are not overloaded, this study aims to establish low impedance paths of DGs, just like passive filters, to absorb as much harmonic currents as possible. The main contributions of this study are as follows.

1) An adaptive HVI control is proposed. Under the assumption that a residual capacity exists, the HVI is adaptively tuned through a fuzzy controller. Unlike existing methods, the proposed control can maximize the utilization of DGs to mitigate harmonics, significantly improving voltage quality.

2) An eigen-value analysis is used to determine the stability domain of the HVI. The effects of harmonic extraction and grid and control parameters on stability are analyzed in detail. A control law of the HVI is then designed to ensure the stability domain.

3) An evaluation based on Monte Carlo harmonic power flow is proposed to demonstrate the effectiveness of the proposed control. Comparative studies using real-time simulations are conducted with two state-of-the-art research works. The performance of the proposed control is tested under both steady and dynamic states.

The remainder of the study is organized as follows. Section II presents basic concept of virtual impedance control. Section III discusses stability domain of HVI, and Section IV presents the proposed control. Sections V and VI present the results of simulations and control-in-the-loop (CIL) experiments, respectively. Finally, Section VII concludes the study and suggests future applications for the proposed control.

II. Basic Concept of Virtual Impedance Control

A. Droop Control

A single-phase microgrid is used to illustrate the proposed control, and the analysis of three-phase systems is similar to that of single-phase systems. When the microgrid is inductive, the active power is mainly affected by the phase angle, whereas the reactive power is mainly related to the voltage magnitude [24]. As a result, droop control is established as:

$$\begin{cases} f = f_n - m(P - P_n) \\ U = U_n - n(Q - Q_n) \end{cases} \tag{1}$$

where f and U are the frequency and magnitude of the output voltage, respectively; f_n and U_n are the rated frequency and magnitude of the output voltage, respectively; P and Q are the output active and reactive power of the inverter, respectively; P_n and Q_n are the rated active and reactive power, respectively; and m and n are the active and reactive power droop coefficients, respectively. Note that the assumption of "inductive" may not always hold, and many advanced droop controls can be used instead [6]-[8].

As the system frequency is uniform in the steady state, different inverters can properly share the active power by setting the droop coefficient to be inversely proportional to the rated capacity. However, the voltage magnitudes measured by inverters are inconsistent due to line impedances, which results in undesirable reactive power sharing. To address this problem, a widely adopted solution is to add virtual impedance [21], and its principle is briefly described as follows.

B. Virtual Impedance Control

Figure 1 shows an inverter block diagram with virtual impedance control $G_{vir}(s)$. A dual-loop control structure is adopted. The voltage outer loop uses multi-resonant quasi-proportional-resonant (quasi-PR) controller $G_{PR}(s)$ [25] to track the output voltage, and the current inner loop employs proportional control $G_d(s)$ to enhance the dynamic performance. Note that the definitions of the undefined variables and parameters in the figures of this study can be found in Supplementary Material A.

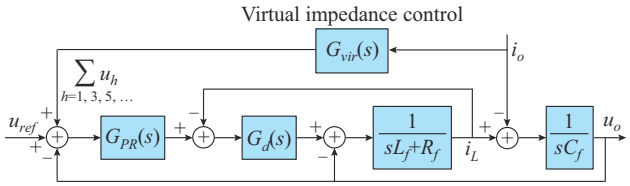

Fig. 1. Inverter block diagram with virtual impedance control $G_{vir}(s)$.

A second-order generalized integrator-quadrature signal generator (SOGI-QSG) [26], [27] is used to extract the fundamental frequency components of the output current i_o, which are $G_{1\alpha}(s)$ and $G_{1\beta}(s)$ expressed as:

$$\begin{cases} G_{1\alpha}(s) = \dfrac{k_1\omega_1 s}{s^2 + k_1\omega_1 s + \omega_1^2} \\ G_{1\beta}(s) = \dfrac{k_1\omega_1^2}{s^2 + k_1\omega_1 s + \omega_1^2} \end{cases} \tag{2}$$

where ω_1 is the fundamental angular frequency; and k_1 is the gain coefficient. The amplitude gain of $G_{1\alpha}(s)$ at the frequency of ω_1 is 1 at a phase angle of 0°. The amplitude gain of $G_{1\beta}(s)$ at the frequency of ω_1 is also 1 but at a phase angle of −90°. After the fundamental components are extracted from i_o through $G_{1\alpha}(s)$ and $G_{1\beta}(s)$, transfer function $G_{vir}(s)$ of the additional virtual impedance control link can be obtained by multiplying different impedance coefficients, as given by:

$$G_{vir}(s) = R_{v1}G_{1\alpha}(s) - \omega_1 L_{v1}G_{1\beta}(s) \tag{3}$$

where R_{v1} and L_{v1} are the virtual resistance and inductance at the fundamental frequency, respectively.

According to Fig. 1, the output voltage $u_o(s)$ of the inverter at the fundamental frequency is expressed as:

$$\begin{cases} u_o(s) = G(s)u_{ref}(s) - Z_{eq}(s)i_o(s) \\ G(s) = \dfrac{G_{PR}(s)G_d(s)}{L_fC_fs^2 + R_fC_fs + C_fG_d(s)s + G_{PR}(s)G_d(s) + 1} \\ Z_{eq}(s) = Z_o(s) + Z_v(s) = \dfrac{sL_f + R_f + G_d(s)}{G_{PR}(s)G_d(s)} \end{cases} \tag{4}$$

where $G(s)$ is the voltage transfer function; $Z_{eq}(s)$ is the equivalent impedance of the inverter; $i_o(s)$ is the output current of the inverter; and $Z_o(s)$ and $Z_v(s)$ are the impedances

of dual-loop and virtual impedance controls, respectively. According to (4), the virtual impedance control can change the value of Z_{vir} without affecting $G(s)$.

C. HVI Control

The working principle of HVI control is similar to virtual impedance control, but an additional step is required to extract harmonic components from the output current. In this study, an SOGI-QSG with a cross-cancellation feedback is used to achieve harmonic current extraction, as shown in Fig. 2. The transfer function corresponding to the harmonic extraction process can be obtained by:

$$\begin{bmatrix} T_{1\alpha}(s) \\ T_{3\alpha}(s) \\ T_{5\alpha}(s) \\ \vdots \end{bmatrix} = \begin{bmatrix} 1 & G_{1\alpha} & G_{1\alpha} & \cdots \\ G_{3\alpha} & 1 & G_{3\alpha} & \cdots \\ G_{5\alpha} & G_{5\alpha} & 1 & \cdots \\ \vdots & \vdots & \vdots & \end{bmatrix}^{-1} \begin{bmatrix} G_{1\alpha} \\ G_{3\alpha} \\ G_{5\alpha} \\ \vdots \end{bmatrix} \tag{5}$$

$$T_{h\beta}(s) = G_{h\beta}(s)\left(1 - \sum_{n \neq h} T_{n\alpha}(s)\right) \tag{6}$$

where $T_{h\alpha}(s)$, $G_{h\alpha}$, $T_{h\beta}(s)$, and $G_{h\beta}(s)$ are the transfer functions of direct (α) and quadrature (β) components of the h^{th} harmonic frequency signal in cross-cancellation SOGI-QSG, respectively.

HVI control can then be implemented as:

$$Z_{vir}(s) = \left(\sum_{h=1,3,5,\ldots} R_{vh} T_{h\alpha}(s) - \sum_{h=1,3,5,\ldots} \omega_h L_{vh} T_{h\beta}(s)\right) G(s) \tag{7}$$

where ω_h is the angular frequency of the h^{th} harmonic frequency signal; R_{vh} and L_{vh} are the harmonic virtual resistance and inductance of the h^{th} harmonic frequency signal, respectively. Figure 2 shows the schematic of an inverter with the proposed control. S_R and S_H are the residual capacity and the harmonic power of the inverter, respectively; and $i_{h\alpha}$ and $i_{h\beta}$ are the extracted harmonic currents, having equal magnitudes with phase angles differing by 90°.

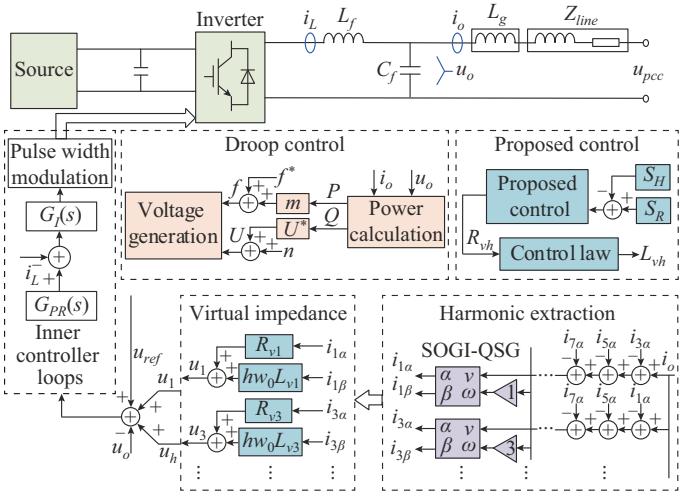

Fig. 2. Schematic of an inverter with proposed control.

III. Stability Domain of HVI

We next analyze the stability domain of HVI in detail, where the findings strongly support the implementation of the proposed control.

A. Stability of a Single Inverter

Figure 3 shows the equivalent circuit of a single inverter, which is represented by a voltage source in series with an equivalent impedance $Z_{eq}(s)$ [22].

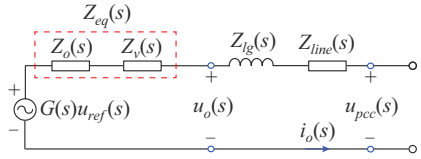

Fig. 3. Equivalent circuit of a single inverter.

From Fig. 3, the relationship between $i_o(s)$ and $u_{pcc}(s)$ can be expressed as:

$$\begin{cases} \dfrac{i_o(s)}{u_{pcc}(s)} = Y(s) = \dfrac{1}{Z_{total}(s)} \\ Z^i_{total}(s) = Z^i_{eq}(s) + Z^i_{lg}(s) + Z^i_{line}(s) \end{cases} \tag{8}$$

where Z^i_{lg} and Z^i_{line} are the grid-side inductance and line impedance, respectively.

Based on the pole distribution of $Y(s)$ in (8), the effect of HVI on the stability of the inverter can be analyzed. Table I lists the parameters of the inverter.

TABLE I
Parameters of Inverter

Parameter	Value
Rated capacity	10 kVA
DC voltage	400
LC filter	$L_f = 1$ mH; $R_f = 0.02$ Ω; $C_f = 30$ μF
Sampling frequency	20 kHz
PR controller	$k_p = 0.05$, $k_{r1} = 20$, $k_{r3} = k_{r5} = k_{r7} = k_{r9} = 15$, $\omega_c = 3$ rad/s
Inner current controller	$k_I = 0.025$
Grid-side inductance	$L_g = 2$ mH
SOGI	$k_1 = 0.1$, $k_3 = k_5 = k_7 = k_9 = 0.02$
Line impedance	$Z_{line} = (0.05 + \text{j}0.005)\Omega$

The pole distributions of $Y(s)$ when R_{vh} and L_{vh} are adjusted separately are shown in Fig. SA1 in Supplementary Material A, and Fig. 4 presents the simulation results of the inverter current when the HVI value changes. The system exists in stable modes at approximately 45 Hz and 470 Hz, respectively.

The instability phenomenon shown in Fig. 4 is investigated in detail using the negative resistance at the resonance frequency [28]. In Fig. 5, the equivalent impedance of the inverter is presented when R_{vh} is fixed at 0 Ω. When L_{vh} is positive, Z_{total} shows a negative resistance below 50 Hz, and the region of the negative resistance gradually expands with an increase in L_{vh}. This phenomenon occurs due to the phase lag property inherent in the harmonic extraction process. As $T_{h\beta}(s)$ lags behind $T_{h\alpha}(s)$ by 90°, when $R_{vh} = 0$ and L_{vh} is positive, $Z_{vir}(s)$ exhibits a negative resistance characteristic based on (7). However, the inductive characteristic of Z_v is more distinct when the crossover cancellation is applied,

which moves the zero-crossing point to the lower frequency. Consequently, the stability domain increases to some extent.

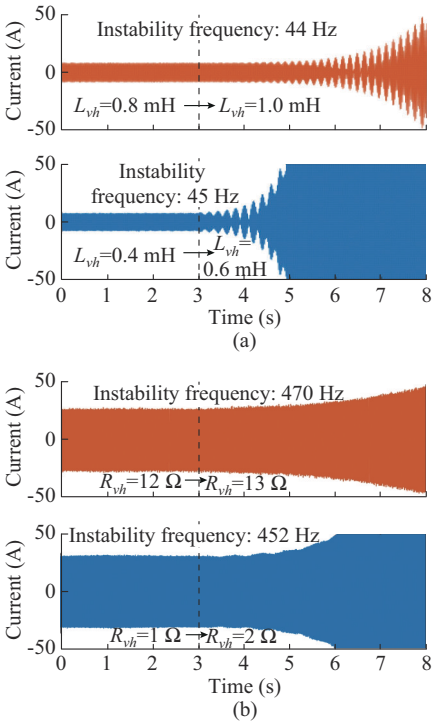

Fig. 4. Simulation results of inverter current when HVI value changes. (a) R_{vh} fixing at 0 Ω and value of L_{vh} changing with crossover cancellation. (b) L_{vh} fixing at –2 mH and value of R_{vh} changing without crossover cancellation.

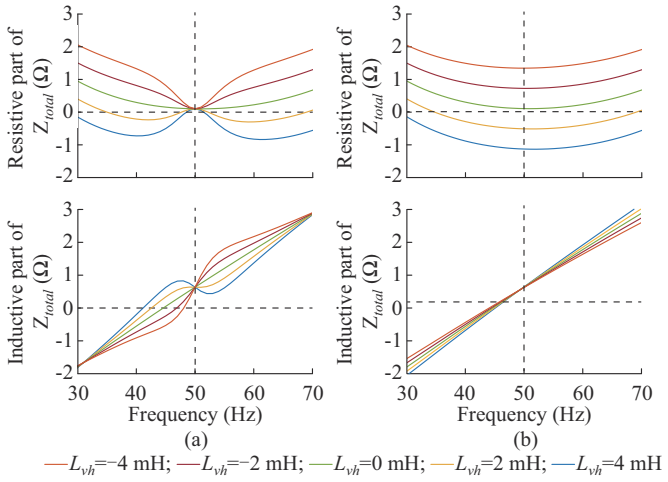

Fig. 5. Resistive and inductive parts of Z_{total} as L_{vh} varies. (a) With crossover cancellation. (b) Without crossover cancellation.

In Fig. 6, the equivalent impedance of the inverter is presented when L_{vh} is fixed at −2 mH to compensate for the grid-side inductance. The negative value of L_{vh} endows Z_v with obvious negative resistance characteristics above 450 Hz, which is the root cause of the 470 Hz oscillation shown in Fig. 6. In addition, the negative resistance of Z_{total}, as shown in Fig. 6(a), is less than that shown in Fig. 6(b), indicating that the stability domain is wider with crossover cancellation.

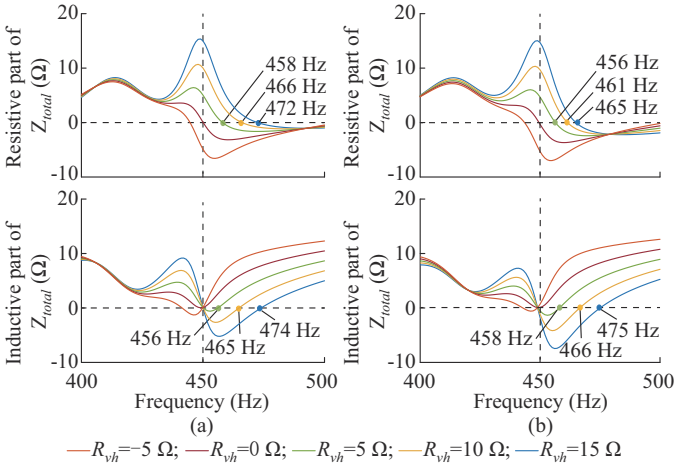

Fig. 6. Resistive and reactive parts of Z_{total} as R_{vh} varies. (a) With crossover cancellation. (b) Without crossover cancellation.

Based on the previous analysis, two conclusions can be drawn: ① crossover cancellation helps to expand the stability domain of HVI control; ② simultaneously increasing R_{vh} and L_{vh} can further expand the stability domain of HVI, as shown in Fig. 7.

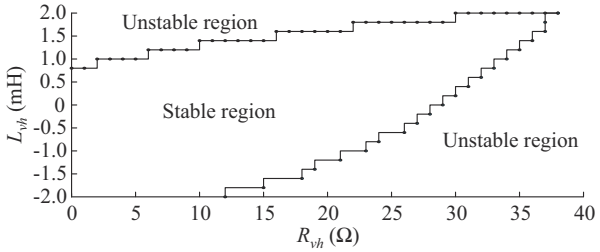

Fig. 7. Stability constraint between R_{vh} and L_{vh}.

B. Sensitivity Study of Stability Domain

The microgrid is subject to various uncertainties that may affect the stability domain of HVI. We next investigate the effects of both grid parameters and control parameters on the stability domain of HVI.

1) Effects of Grid Parameters

According to (8), variations in grid-side inductance L_g and resistance R_L will modify Z_{total} and in turn influence the stability domain. Figure 8 shows the stability domains of HVI under different grid parameters. As shown in Fig. 8, the upper limit of R_{vh} increases with L_g, and the lower limit of L_{vh} also increases to the negative value of the grid-side inductance, i.e., $-L_g$. With the increase in R_L, the upper limit of the stability domain increases, whereas the lower limit remains essentially unchanged.

2) Effects of Control Parameters

The control parameters of the voltage/current loops determine $G(s)$ of the inverter, which in turn influences the stability domain of HVI. Figure 9 presents stability domains of HVI under different control parameters. $G_{PR}(s)$ primarily affects the upper limit of L_{vh}. As $G_{PR}(s)$ decreases, the upper limit of L_{Vh} increases. However, the proportional coefficient of $G_d(s)$ primarily dictates the upper limit of R_{vh}. It can be observed that the upper limit of R_{vh} increases with $G_d(s)$.

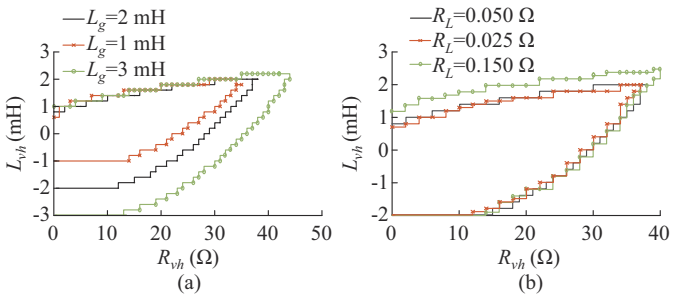

Fig. 8. Stability domains of HVI under different grid parameters. (a) Various grid-side inductances. (b) Various branch resistances.

As Figs. 8 and 9 illustrate, the stability domain of HVI varies under both grid and control parameters. However, in all scenarios, simultaneous adjustment of R_{vh} and L_{vh} helps expand the stability domain. In practical operation, multiple inverters are connected in parallel, as shown in Fig. 10, where $Z_L(s)$ is the equivalent impedance of the remaining part of the system, excluding inverter i. Thus, the stability of the microgrid is determined by both $Z_{total}(s)$ and $Z_L(s)$. Under the steps described in Section III-A, stability analysis can be performed. Notably, the stability domain defined by $Z_{total}(s)$ of a single inverter typically suffices, as $Z_L(s)$ is much smaller than $Z_{total}(s)$ and thus its effect on stability is limited.

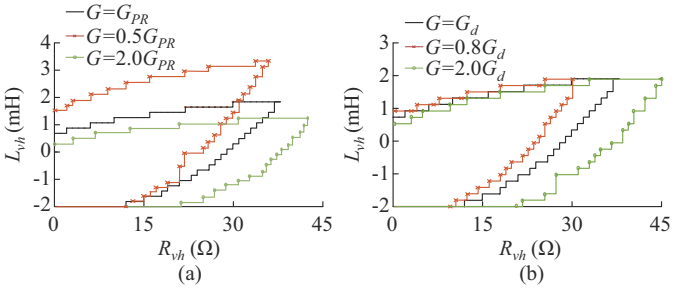

Fig. 9. Stability domains of HVI under different control parameters. (a) Various voltage control parameters. (b) Various current control parameters.

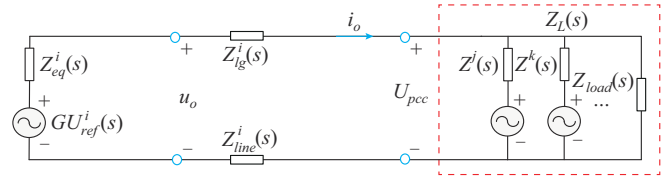

Fig. 10. Equivalent circuit model of multiple inverters connected in parallel.

IV. Proposed Control

A. Adaptive HVI Control

Installing passive filters near harmonic sources has always been effective in improving voltage quality, as the filter provides new paths with small impedances to absorb harmonics. This means that when an inverter close to nonlinear loads has sufficient residual capacity, it is desirable that the inverter should be endowed with a small impedance to create a low impedance path that allows the inverter to absorb more harmonic currents. Based on this idea, a novel adaptive HVI control is proposed in this study. The proposed control dynamically adjusts the HVI through the real-time detection of the residual capacity of the inverter and the harmonic power it consumes. The control objective is to realize a reasonable allocation of harmonic power and improve the power quality performance based on the premise that no inverter is overloaded. The core idea of the proposed control can be expressed as:

$$\begin{cases} R_{vh} = R_{\max} - \dfrac{k_{vi}}{s}(S_R - S_H) \\ L_{vh} = f(R_{vh}) \end{cases} \tag{9}$$

where $R_{\max}$ is the upper limit of virtual resistance; k_{vi} is the integral coefficient; and $f(R_{vh})$ is the control law of L_{vh} and R_{vh}. $R_{\max}$ and $f(R_{vh})$ can be designed based on the stability domain results described in Section III. S_R and S_H can be calculated by referring to [29]:

$$\begin{cases} S_R = \sqrt{S_N^2 - (P^2 + Q^2)} \\ S_H \approx U_{1,rms}\sqrt{\sum_{h=3,5,7,9} I_{h,rms}^2} \end{cases} \tag{10}$$

where S_N is the rated capacity of the inverter; and $U_{1,rms}$ and $I_{h,rms}$ are the root-mean-square (RMS) values of the fundamental voltage and harmonic current, respectively. According to (10), when $S_R > S_H$, R_{vh} and L_{vh} continually decrease, and S_H rises constantly until $S_R = S_H$. If S_R is considerably greater than S_H, R_{vh} and L_{vh} decrease to the minimum, which effectively improves the voltage quality. When the load demand increases, resulting in $S_R < S_H$, R_{vh} and L_{vh} continue to increase until $S_R = S_H$, thereby ensuring that the inverter does not overload. Therefore, effective voltage quality enhancement can be achieved without overloading.

B. Fuzzy Integral Controller

As the power calculation in (10) is highly nonlinear, selecting an appropriate integral coefficient k_{vi} in (9) is crucial. If k_{vi} is too large, the control system loses its stability, whereas a is too small k_{vi} results in poor dynamic performance. Fuzzy control is a method based on fuzzy logic theory and is suitable for systems with unknown mathematical models and strong nonlinearities [30], [31]. It allows fuzzy membership functions and fuzzy rules to be set based on different model characteristics and human expertise, thus offering good robustness and dynamic performance. This study constructs a two-input one-output fuzzy controller to determine the value of k_{vi}. The inputs of the controller consist of the error $e(t)$ between S_R and S_H and its rate of change, as expressed by:

$$\begin{cases} e(t) = \dfrac{S_R(t) - S_H(t)}{S_N} \\ \Delta e = \dfrac{e(n\Delta t) - e(n\Delta t - \Delta t)}{\Delta t} \end{cases} \tag{11}$$

where $e(n\Delta t)$ is the error sampled at the n^{th} instant; and Δt is the sampling time. The fuzzy rules are defined as R_i, if e is E_i and Δe is ΔE_i, $k_{vi} = K_i$, $i = 1, 2, \ldots, M$. M is the number of fuzzy rules; E_i and ΔE_i are the membership functions for the inputs e and Δe in the i^{th} rule, respectively; and K_i is the membership function for k_{vi} in the i^{th} rule. The membership

functions of $e(t)$, Δe, and K_i are defined on a common normalized domain $[-3,3]$. The baseline values for $e(t)$, Δe, and K_i are 0.05, 0.05, and 150, respectively. A simplified triangular membership function is adopted for control, as shown in Fig. 11, where NL, NM, NS, Z, PS, PM, and PL denote negative large, negative medium, negative small, zero, positive small, positive medium, and positive large, respectively.

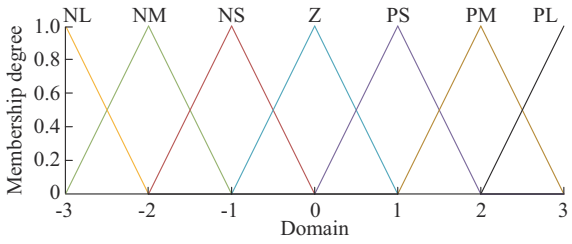

Fig. 11. Membership function of $e(t)$, Δe, and k_{vi}.

Based on the design method described in [31], the fuzzy control rules for adjusting K_i in this study mainly consider the following two aspects:

1) When $\Delta e \cdot e > 0$, $|e|$ continuously increases, indicating that the difference between S_R and S_H gradually increases. In this case, k_{vi} should be increased to accelerate the adjustment rate of the HVI.

2) When $\Delta e \cdot e < 0$, $|e|$ continuously decreases. If e is a small value and Δe is large, k_{vi} should be reduced or even made negative to suppress the rate of change and prevent oscillations. By contrast, k_{vi} should be increased to accelerate the adjustment rate of the HVI.

Based on the aforementioned aspects, 49 fuzzy rules, indicated by the superscript, are designed in this study, as listed in Table II. Finally, the center-of-gravity method is employed for defuzzification, as expressed by:

$$k_{vi} = \frac{\sum_{i=1}^{M} u(e)_i u(\Delta e)_i K_i}{\sum_{i=1}^{M} u(e)_i u(\Delta e)_i} \tag{12}$$

where $u(e)_i$ is the membership degree of $e(t)$ in the i^{th} rule; and $u(\Delta e)_i$ is the membership degree of Δe in the i^{th} rule.

TABLE II
RULES OF FUZZY CONTROL

Derivative of error	Error						
	NL	NM	NS	Z	PS	PM	PL
NL	PL^{1}	PL^{2}	PM^{3}	NL^{4}	NM^{5}	PS^{6}	PS^{7}
NM	PL^{8}	PM^{9}	PM^{10}	Z^{11}	NS^{12}	PS^{13}	PS^{14}
NS	PM^{15}	PS^{16}	PS^{17}	Z^{18}	PS^{19}	PS^{20}	PM^{21}
Z	PM^{22}	PS^{23}	PS^{24}	Z^{25}	PS^{26}	PS^{27}	PM^{28}
PS	PM^{29}	PS^{30}	PS^{31}	Z^{32}	PS^{33}	PS^{34}	PM^{35}
PM	PS^{36}	PS^{37}	NS^{38}	Z^{39}	PM^{40}	PM^{41}	PL^{42}
PL	PS^{43}	PS^{44}	NM^{45}	NL^{46}	PM^{47}	PL^{48}	PL^{49}

C. Evaluation Based on Monte Carlo Harmonic Power Flow

When all inverters in the microgrid are designed with the proposed control, the final steady state is that the HVI of each inverter reaches the minimum allowable value, and multiple low harmonic impedance paths are constructed to absorb harmonic currents in the microgrid, as with passive filters. However, this method does not guarantee that the voltage quality improvement is optimal, as its performance depends on the microgrid topology and the objective function, and generally an optimization algorithm is required. The idea here is inspired by field experiences. And the paths with small impedances are added, which in most cases, help improve power quality. For a rigorous evaluation of the effectiveness of the proposed control, an evaluation based on Monte Carlo harmonic power flow is introduced. The specific steps of this evaluation are as follows.

Step 1: initialization. Determine the number of total inverters n, the number of inverters k with the proposed control, the HVI range $[Z_{\min}, Z_{\max}]$, the control law of L_{vh} and R_{vh}, the impedance change step r, and the maximum number of iterations $N_{\max}$.

Step 2: establish the node admittance matrix of the microgrid and the harmonic models of nonlinear loads.

Step 3: select one inverter as the target inverter.

Step 4: randomly sample the HVI of the remaining $k-1$ inverters within the feasible range.

Step 5: change the HVI of the target inverter from small to large in increments of r and evaluate the voltage quality using harmonic power flow.

Step 6: return to *Step 4* and generate another operation condition. If sufficient operation conditions are generated for a certain target inverter, proceed to *Step 7*.

Step 7: return to *Step 3* and select another inverter as the target inverter. If all inverters have been evaluated, the performance evaluation is completed.

For all operation conditions, if the voltage quality improves with a decrease in the HVI of the target inverter, it means that the proposed control is effective, as a small HVI always leads to improved voltage quality.

V. CASE STUDY

A. System Description

To validate the effectiveness of the proposed control, a multi-bus microgrid is built in MATLAB/Simulink [32], as shown in Fig. SB1 in Supplementary Material B. Tables I and III list the simulation parameters of the microgrid. The rated power of linear load of Buses 1-6 is 5.5 kW+j2 kvar.

TABLE III
SYSTEM SIMULATION PARAMETERS

Parameter	Value of Inverters 1, 2, and 5	Value of Inverters 3, 4
Rated capacity	10 kVA	5 kVA
Droop coefficient	10^{-5}	2×10^{-5}
Voltage controller	$k_p=0.05$; $k_{r1}=20$; $\omega_c=3$ rad/s; $k_{r3}=k_{r5}=k_{r7}=k_{r9}=15$	$k_p=0.025$; $k_{r1}=10$; $\omega_c=3$ rad/s; $k_{r3}=k_{r5}=k_{r7}=k_{r9}=7.5$
Current controller	$k_I=0.025$	$k_I=0.05$
Grid-side inductance	$L_g=2$ mH	$L_g=3$ mH

Figure 12 shows the stability domains of different inverters. It shows that the stability domain shrinks with an increase in $R_{\max}$. Therefore, $R_{\max}$ should not be excessively large. In this study, $R_{\max}$ is set to be 20 Ω. To reduce the computational burden, a linear function is designed to express the control law. To maximize the stability domain, $f_1(R_{vh})$ and $f_2(R_{vh})$ are defined as $-2(1-R_{vh}/R_{\max})$ and $-3(1-R_{vh}/R_{\max})$, respectively.

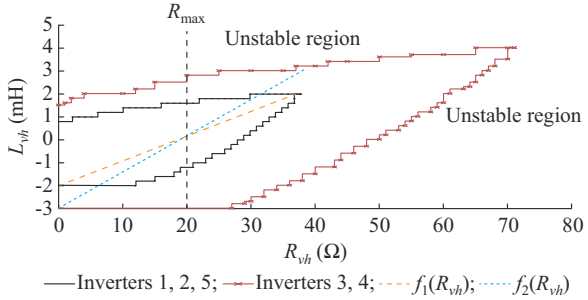

Fig. 12. Stability domains of different inverters.

B. Performance Evaluation

Before the proposed control is applied, an evaluation based on Monte Carlo harmonic power flow is conducted. Figure 13 shows the variation of the voltage of the total harmonic distortion (THD) U_{THD} with HVI of Inverter 2. The simulated harmonic distortions at Buses 4 and 6 with Inverter 2 as the target inverter are illustrated. Each line in the figure represents an operation condition in which HVIs for Inverters 1, 3, 4, and 5 are randomly generated and then fixed, whereas the HVI of Inverter 2 varies from small to large. A total of 2000 operation conditions is evaluated.

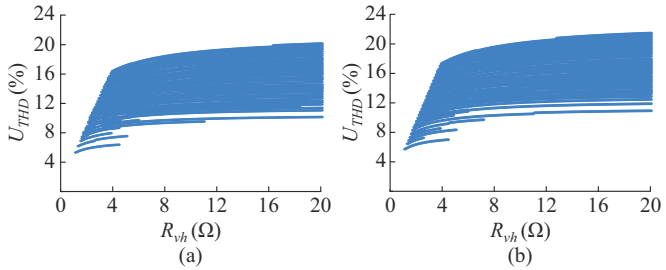

Fig. 13. Variation of U_{THD} with HVI of Inverter 2. (a) Bus 4. (b) Bus 6.

As Fig. 13 shows, the voltage distortion increases with the HVI of Inverter 2, indicating that in this microgrid, reducing the impedance of Inverter 2 always improves the voltage quality. The aforementioned evaluation is repeated for other inverters, and similar conclusions can be drawn. Thus, the effectiveness of the proposed control is confirmed.

C. EMTP Simulation Results

Figure 14 shows the voltage waveform of Bus 6 before and after the application of the proposed control. Before applying the proposed control, the THD of Bus 6 voltage is 7.49%. The value decreases to 4.18% after the proposed control is applied, demonstrating a notable improvement in voltage quality.

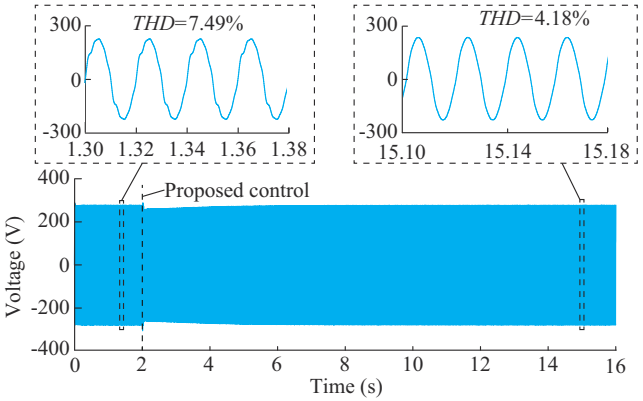

Fig. 14. Voltage waveform of Bus 6 before and after applying proposed control.

Table IV and Fig. SB2 in Supplementary Material B show the changes in S_R and S_H for different inverters. It should be noted that Inverters 3 and 4 become overloaded due to excessive harmonic power absorption before applying the proposed control, whereas Inverters 1, 2, and 5 still have the capacity for additional harmonic power, indicating an unreasonable harmonic power allocation at this time. After the proposed control is applied at 2 s, the harmonic power of Inverters 1, 2, and 5 increases. In addition, the harmonic power of Inverters 3 and 4 gradually decreases. Finally, all inverters nearly reach the state of $S_H = S_R$. Therefore, a reasonable harmonic power allocation is reached with various inverters. Table V compares the THDs of Buses 1-6. It shows that with the proposed control, the voltage quality of the microgrid is significantly improved due to the low-impedance path provided by the inverters.

TABLE IV
VARIATIONS IN RESIDUAL CAPACITY AND HARMONIC POWER OF INVERTERS

Inverter	Before applying proposed control (p.u.)		After applying proposed control (p.u.)	
	S_R	S_H	S_R	S_H
Inverter 1	0.1465	0.1292	0.1555	0.1538
Inverter 2	0.1515	0.1286	0.1614	0.1593
Inverter 3	0.1541	0.1687	0.1590	0.1561
Inverter 4	0.1502	0.1676	0.1567	0.1546
Inverter 5	0.1484	0.1284	0.1569	0.1556

TABLE V
VOLTAGE QUALITY IMPROVEMENTS OF DIFFERENT BUSES

Bus	*THD* (%)	
	Before applying proposed control	After applying proposed control
Bus 1	7.23	3.53
Bus 2	7.19	3.48
Bus 3	7.31	3.68
Bus 4	7.33	3.77
Bus 5	7.17	3.48
Bus 6	7.49	4.18

D. Harmonic Mitigation: Proposed Control vs. Decentralized Control

Reference [21] proposed a decentralized control called negative virtual harmonic impedance (NVH-Z) control, which is expressed by (13). Essentially, the decentralized control adds a negative HVI to change the effective line impedance at harmonic frequencies. Consequently, the decentralized control addresses the problem of uneven harmonic power distribution among inverters caused by line impedance mismatch. Besides, it considers power quality improvement.

$$Z_{vh} = Z_h^* - b(S_R - S_H) \tag{13}$$

where Z_{vh} is the added HVI; Z_h^* is the added HVI at the full load, which is generally 0; and b is a droop coefficient. When a proper b is specified for different inverters, Z_{vh} can be adjusted to address the line impedance mismatch and thus achieve harmonic sharing. In addition, because Z_{vh} is negative, line impedance is reduced, and the power quality is improved to some extent. For a comparative study, the NVH-Z control is applied to the system shown in Fig. SB1 in Supplementary Material B. The variations in S_R and S_H of different inverters under the NVH-Z control are shown in Fig. SB3 in Supplementary Material B. Table VI compares the voltage quality under the two control strategies. As the table shows, the proposed control outperforms NVH-Z control and thus more effectively utilizes inverter capacity to improve voltage quality.

TABLE VI
COMPARISON OF VOLTAGE QUALITY UNDER NVH-Z CONTROL AND PROPOSED CONTROL

Bus	*THD* (%)		
	Before applying proposed control	Proposed control	NVH-Z control
Bus 1	7.23	3.53	6.71
Bus 2	7.19	3.48	6.65
Bus 3	7.31	3.68	6.80
Bus 4	7.33	3.77	6.83
Bus 5	7.17	3.48	6.66
Bus 6	7.49	4.18	6.95

E. Harmonic Mitigation: Proposed Control vs. Centralized Control

To further evaluate its effectiveness, the proposed control is compared with the centralized control proposed in [19]. Figure SB1 in Supplementary Material B formulates an optimization problem for the microgrid, the goal of which is to minimize the average harmonic distortions of all buses, with virtual impedances of inverters used as variables. The problem can be solved using the improved comprehension learning particle swarm optimization algorithm [33]. The voltage waveforms of Bus 6 under two controls are shown in Fig. SB4 in Supplementary Material B. Table VII compares the voltage quality under centralized control and proposed control.

Table VII shows that the improvement in voltage quality under the proposed control is less than that of the centralized control. To explain this, the control law restriction (i.e., $f_1(R_{vh}) = -2(1 - R_{vh}/R_{\max})$ and $f_2(R_{vh}) = -3(1 - R_{vh}/R_{\max})$) is added to the centralized control. Table VIII presents the voltage quality performances of the proposed control and centralized control with control law restriction. As the table shows, the voltage performance of the centralized control is very similar to that of the proposed control.

TABLE VII
COMPARISON OF VOLTAGE QUALITY UNDER CENTRALIZED CONTROL AND PROPOSED CONTROL

Bus	*THD* (%)		
	Before applying proposed control	Proposed control	Centralized control
Bus 1	7.23	3.53	3.01
Bus 2	7.19	3.48	2.94
Bus 3	7.31	3.68	3.14
Bus 4	7.33	3.77	3.19
Bus 5	7.17	3.48	2.94
Bus 6	7.49	4.18	3.61

TABLE VIII
VOLTAGE QUALITY PERFORMANCES OF PROPOSED CONTROL AND CENTRALIZED CONTROL WITH CONTROL LAW RESTRICTION

Bus	*THD* (%)	
	Proposed control	Centralized control with control law restriction
Bus 1	3.53	3.41
Bus 2	3.48	3.37
Bus 3	3.68	3.56
Bus 4	3.77	3.65
Bus 5	3.48	3.35
Bus 6	4.18	4.10

Table IX shows the HVIs under various controls. According to Tables VII-IX, it is confirmed that the addition of control law restrictions results in different HVIs for the centralized control, thereby degrading the voltage quality performance. In other words, the control law designed in this study is not optimal. However, this result is acceptable, as the proposed control enables efficient harmonic mitigation without relying on communication.

TABLE IX
HVIS UNDER VARIOUS CONTROLS

Inverter	HVI					
	Proposed control		Centralized control		Centralized control with control law restriction	
	Re	Im	Re	Im	Re	Im
Inverter 1	0.979	–0.597	0.630	–0.511	0.935	–0.599
Inverter 2	0.929	–0.599	0.574	–0.511	0.903	–0.600
Inverter 3	1.914	–0.852	1.291	–0.691	1.891	–0.853
Inverter 4	1.971	–0.849	1.400	–0.721	1.953	–0.850
Inverter 5	0.957	–0.598	0.619	–0.513	0.936	–0.599

F. Dynamic Performance

To verify the performance of the proposed control under sudden changes in the operation state, load switching experiments are conducted. The linear load on Bus 6 is cut off at 4 s and then switched on again at 8 s.

To demonstrate the usefulness of the fuzzy control, Fig. 15 shows the simulation results in three scenarios, including the designed fuzzy integral controller and fixed integral gain at $k_{vi}=50$ and $k_{vi}=150$. Due to space limitations, only the results for Inverters 1-3 are presented here. Figure 15 shows that the HVI of the inverter can quickly reach a stable state under the fuzzy control, and the voltage quality can also be rapidly improved. When the integral parameter k_{vi} is fixed at 50, the HVIs of the inverters respond slowly, which means the dynamic performance is unsatisfactory. When k_{vi} is fixed at 150, the HVIs and harmonic power of the inverters oscillate considerably, which causes the bus voltage distortion to fluctuate periodically and affects the normal operation of the microgrid. These results show that the fuzzy integral controller strikes a good balance between convergence performance and the speed of dynamic response.

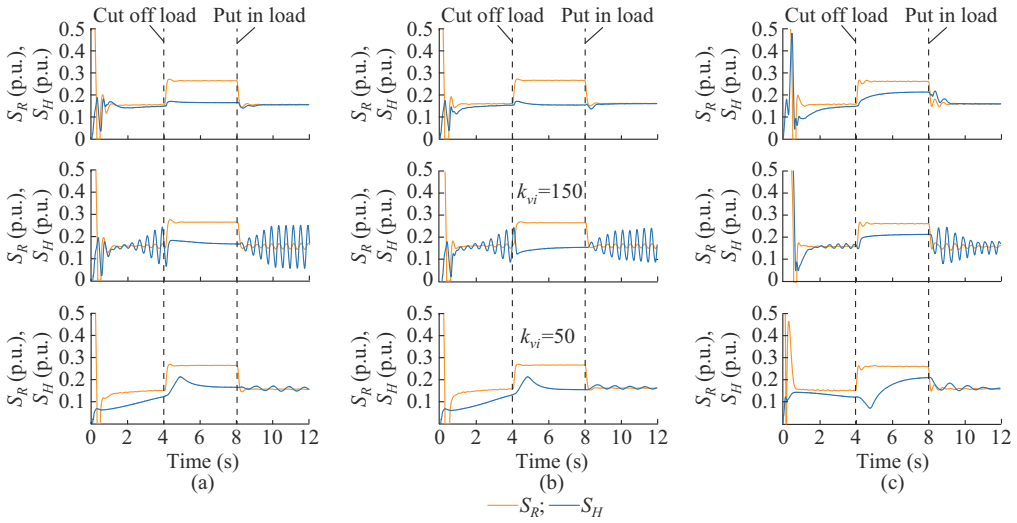

Fig. 15. Variations in S_R and S_H of Inverters 1-3 during resistive load switching. (a) Inverter 1. (b) Inverter 2. (c) Inverter 3.

VI. CIL Experiments

The CIL combines physical and virtual test (real controllers plus virtual objects) and has been widely used to validate the controllers of power electronic device [34]. A CIL experiment uses real-time processors to run simulation models that mimic the operation states of the controlled objects. Real-time processors connect to the tested controller through an I/O interface, allowing for comprehensive system test. The model of the test circuit is developed in the simulation software StarSim and runs on MT6020, as shown in Fig. SC1 in Supplementary Material C. The proposed control is implemented on MT1050. The analog/digital signals are channeled through the I/O board between MT6020 and MT1050, forming a closed loop. The inverter parameters are consistent with those described in Section V, and the line parameters are listed in Table X.

As Fig. SC2 in Supplementary Material C shows, the voltage quality of Bus 4 is improved when the proposed control is applied. The THD is reduced from 8.04% to 3.97%. Table XI compares the voltage THD before and after applying the proposed control. Figure SC3 in Supplementary Material C shows the variations in residual capacity and harmonic power of different inverters. As the figure shows, the proposed control effectively prevents inverter overload. Next, load switching experiments are conducted, where the results for Inverter 3 are presented in Fig. SC4 in Supplementary Material C. When $k_{vi}=800$, the harmonic power of Inverter 3 oscillates. When $k_{vi}=50$ or the fuzzy control is adopted, the inverter can realize the desired control performance, but the fuzzy control leads to a faster dynamic response. These experimental results validate the feasibility of the proposed control.

TABLE X
Line Parameters

Parameter	Value
Line impedance	$Z_{line}=2\times(0.0261+\mathrm{j}0.0024)\,\Omega$
Linear loads 1 and 2	$L=40$ mH, $R=3\,\Omega$
Linear load 3	$L=35$ mH, $R=5\,\Omega$
Linear load 4	$L=0$ mH, $R=21\,\Omega$
Linear load 5	$L=5$ mH, $R=5\,\Omega$
Nonlinear load 2	$R_1=1\,\Omega$, $C=20$ mF, $R_2=15\,\Omega$
Nonlinear load 1	$R_1=1\,\Omega$, $C=10$ mF, $R_2=30\,\Omega$

TABLE XI
Voltage THD Before and After Applying Proposed Control

Bus	*THD* (%)	
	Before applying proposed control	After applying proposed control
Bus 1	7.83	3.66
Bus 2	7.90	3.74
Bus 3	8.06	4.01
Bus 4	8.04	3.97

VII. Conclusion

This study presents an adaptive HVI control for improving the voltage quality of microgrids. With the residual capacity used as the input and HVI as the output, the output impedance of all DGs can be minimized without experiencing overloading. These low impedance branches filter harmonic currents and then improve the voltage quality. The stability of the proposed control is comprehensively studied, where the results indicate that simultaneously adjusting the resistive and inductive parts of the HVI effectively expands the stability domain. In addition, a fuzzy controller is utilized to enhance the dynamic performance.

The proposed control is expected to be applied to situations in which low-order harmonics caused by nonlinear loads are a concern and precise harmonic sharing is not mandatory. A comparison with two state-of-the-art control strategies demonstrates the advantages of the proposed control. The study also demonstrates that the control law of HVI is critical in improving voltage quality and must be carefully designed in practice. Finally, it should be noted that achieving optimal voltage quality with the proposed control is not guaranteed, as this depends on the microgrid topology and objective function. Typically, such optimal voltage quality necessitates a global optimization strategy, supported by effective communication. However, the performance of the proposed control, as revealed in the detailed case study verification, is still satisfactory. In addition, an evaluation based on Monte Carlo harmonic power flow is proposed, which can be used in practice to demonstrate the applicability of the proposed control.

References

[1] M. H. Saeed, F. Wang, and B. A. Kalwar *et al*., "A review on microgrids' challenges & perspectives," *IEEE Access*, vol. 9, pp. 166502-166517, Feb. 2021.

[2] L. Yan, M. Sheikholeslami, W. Gong *et al*, "Architecture, control, and implementation of networked microgrids for future distribution systems," *Journal of Modern Power Systems and Clean Energy*, vol. 10, no. 2, pp. 286-299, Mar. 2022.

[3] S. Parhizi, H. Lotfi, A. Khodaei *et al*., "State of the art in research on microgrids: a review," *IEEE Access*, vol. 3, pp. 890-925, Jun. 2015.

[4] H. K. Morales-Paredes, J. P. Bonaldo, and J. A. Pomilio, "Centralized control center implementation for synergistic operation of distributed multifunctional single-phase grid-tie inverters in a microgrid," *IEEE Transactions on Industrial Electronics*, vol. 65, no. 10, pp. 8018-8029, Oct. 2018.

[5] E. Espina, J. Llanos, C. Burgos-Mellado *et al*., "Distributed control strategies for microgrids: an overview," *IEEE Access*, vol. 8, pp. 193412-193448, Jun. 2020.

[6] H. Han, X. Hou, J. Yang *et al.*, "Review of power sharing control strategies for islanding operation of AC microgrids," *IEEE Transactions on Smart Grid*, vol. 7, no. 1, pp. 200-215, Jan. 2016.

[7] M. Malakondaiah, K. K. Boddeti, B. R. Naidu *et al.*, "Second harmonic voltage injection-based self impedance estimation for effective decoupled droop control in a microgrid," *Energy Conversion and Economics*, vol. 3, no. 4, pp. 227-243, Aug. 2022.

[8] R. Wang, Q. Sun, Y. Gui *et al*., "Exponential-function-based droop control for islanded microgrids," *Journal of Modern Power Systems and Clean Energy*, vol. 7, no. 4, pp. 899-912, Jul. 2019.

[9] S. K. Panda and B. Subudhi, "A review on robust and adaptive control schemes for microgrid," *Journal of Modern Power Systems and Clean Energy*, vol. 11, no. 4, pp. 1027-1040, Jul. 2023.

[10] S. Haider, G. Li, and K. Wang, "A dual control strategy for power sharing improvement in islanded mode of AC microgrid," *Protection and Control of Modern Power Systems*, vol. 3, no. 1, p. 10, Apr. 2018.

[11] A. S. Vijay, N. Parth, S. Doolla *et al*., "An adaptive virtual impedance control for improving power sharing among inverters in islanded AC microgrids," *IEEE Transactions on Smart Grid*, vol. 12, no. 4, pp. 2991-3003, Jul. 2021.

[12] B. Gao, Y. Wang, and W. Xu, "An improved model of voltage source converters for power system harmonic studies," *IEEE Transactions on Power Delivery*, vol. 37, no. 4, pp. 3051-3061, Aug. 2022.

[13] S. K. Bilgundi, R. Sachin, H. Pradeepa *et al*., "Grid power quality enhancement using an ANFIS optimized PI controller for DG," *Protection and Control of Modern Power Systems*, vol. 7, no. 1, p. 1-3, Jan. 2022.

[14] X. Xiao, Z. Li, Y. Wang *et al*., "A practical approach to estimate harmonic distortions in residential distribution system," *IEEE Transactions on Power Delivery*, vol. 36, no. 3, pp. 1418-1427, Jun. 2021.

[15] Y. Han, H. Li, P. Shen *et al.*, "Review of active and reactive power sharing strategies in hierarchical controlled microgrids," *IEEE Transactions on Power Electronics*, vol. 32, no. 3, pp. 2427-2451, Mar. 2017.

[16] D. De and V. Ramanarayanan, "Decentralized parallel operation of inverters sharing unbalanced and nonlinear loads," *IEEE Transactions on Power Electronics*, vol. 25, no. 12, pp. 3015-3025, Dec. 2010.

[17] Z. Wang, Y. Chen, X. Li *et al*., "Impedance-based adaptively reshaping method for enhancing nonlinear load sharing and voltage quality in islanded microgrids with virtual synchronous generator," *IEEE Transactions on Smart Grid*, vol. 13, no. 4, pp. 2568-2578, Apr. 2022.

[18] T. V. Hoang and H. -H. Lee, "Virtual impedance control scheme to compensate for voltage harmonics with accurate harmonic power sharing in islanded microgrids," *IEEE Journal of Emerging and Selected Topics in Power Electronics*, vol. 9, no. 2, pp. 1682-1695, Feb. 2021.

[19] X. Xiao, Z. Li, Y. Wang *et al*., "Optimal power quality compensation of energy storage system in distribution networks based on unified multi-phase OPF model," *IEEE Transactions on Smart Grid*, vol. 13, no. 3, pp. 1873-1887, Mar. 2022.

[20] H. Dong, S. Yuan, and Z. Han, "A comprehensive strategy for power quality improvement of multi-inverter-based microgrid with mixed loads," *IEEE Access*, vol. 6, pp. 30903-30916, Jan. 2018.

[21] V. Sreekumar and V. Khadkikar, "A new virtual harmonic impedance scheme for harmonic power sharing in an islanded microgrid," *IEEE Transactions on Power Delivery*, vol. 31, no. 3, pp. 936-945, Jun. 2016.

[22] P. Sreekumar and V. Khadkikar, "Direct control of the inverter impedance to achieve controllable harmonic sharing in the islanded microgrid," *IEEE Transactions on Industrial Electronics*, vol. 64, no. 1, pp. 827-837, Jan. 2017.

[23] Z. Zeng, H. Yi, H. Zhai *et al*., "Harmonic power sharing and PCC voltage harmonics compensation in islanded microgrids by adopting virtual harmonic impedance method," in *Proceedings of IECON 2017–43rd Annual Conference of the IEEE Industrial Electronics Society*, Beijing, China, Aug. 2017, pp. 263-267.

[24] P. Li, X. Wang, W. J. Lee *et al*., "Dynamic power conditioning method of microgrid via adaptive inverse control," *IEEE Transactions on Power Delivery*, vol. 30, no. 2, pp. 906-913, Apr. 2015.

[25] W. Sou, C. Chao, C. Gong *et al*., "Analysis, design, and implementation of multi-quasi-proportional-resonant controller for thyristor-controlled LC-coupling hybrid active power filter (TCLC-HAPF)," *IEEE Transactions on Industrial Electronics*, vol. 69, no. 1, pp. 29-40, Jan. 2022.

[26] J. M. Alcala, M. Castilla, L. G. de Vicuña *et al*., "Virtual impedance loop for droop-controlled single-phase parallel inverters using a second-order general-integrator scheme," *IEEE Transactions on Power Electronics*, vol. 25, no. 12, pp. 2993-3002, Dec. 2010.

[27] P. Rodríguez, A. Luna, I. Candela *et al*., "Multiresonant frequency-locked loop for grid synchronization of power converters under distorted grid conditions," *IEEE Transactions on Industrial Electronics*, vol. 58, no. 1, pp. 127-138, Jan. 2011.

[28] H. Liu, X. Xie, C. Zhang *et al*., "Quantitative SSR analysis of series-compensated DFIG-based wind farms using aggregated RLC circuit model," *IEEE Transactions on Power Systems*, vol. 32, no. 1, pp. 474-483, Jan. 2017.

[29] *IEEE Standard Definitions for the Measurement of Electric Power Quantities Under Sinusoidal, Balanced or Unbalanced Conditions*, IEEE Standard 1459-2010.

[30] X. Duan, H. Deng, and H. Li, "A saturation-based tuning method for fuzzy PID controller," *IEEE Transactions on Industrial Electronics*, vol. 60, no. 11, pp. 5177-5185, Nov. 2013.

[31] A. Luo, C. Tang, Z. Shuai *et al*., "Fuzzy-PI-based direct-output-voltage control strategy for the STATCOM used in utility distribution systems," *IEEE Transactions on Industrial Electronics*, vol. 56, no. 7, pp. 2401-2411, Jul. 2009.

[32] S. Papathanassiou, N. Hatziargyriou, and K. Strunz, "A benchmark low voltage microgrid network," in *Proceedings of the CIGRE Symposium: Power Systems with Dispersed Generation*, Athens, Greece, Apr. 2005, pp. 1-8.
[33] Z. Wang, Z. Zhan, and J. Zhang, "An improved method for comprehensive learning particle swarm optimization," in *Proceedings of 2015 IEEE Symposium Series on Computational Intelligence*, Cape Town, South Africa, Aug. 2015, pp. 218-225.
[34] X. Huang, K. Wang, B. fan *et al*., "Robust current control of grid-tied inverters for renewable energy integration under non-ideal grid conditions," *IEEE Transactions on Sustainable Energy*, vol. 11, no. 1, pp. 477-488, Jan. 2020.

Yang Wang received the B.S. degree in electrical engineering from Zhejiang University, Hangzhou, China, in 2012, and the Ph.D. degree in electrical and computer engineering from the University of Alberta, Edmonton, Canada, in 2017. He is currently a Research Fellow with the College of Electrical Engineering, Sichuan University, Chengdu, China. He is the Editor of the IEEE Transactions on Power Delivery and IEEE Open Access Journal of Power and Energy. His main research interests include power quality and integration of renewable.

Xiang Zhou received the B.S. degree in electrical engineering from Sichuan University, Chengdu, China, in 2022. He is currently pursuing the M.S. degree with the College of Electrical Engineering, Sichuan University, Chengdu, China. His current research interests include power quality and control of power electronic converters.

Junming Tang received the B. S. degree in electrical engineering from Ningbo University, Ningbo, China, in 2020. She is currently pursuing the M.S. degree with the College of Electrical Engineering, Sichuan University, Chengdu, China. Her current research interests include power quality and control of power electronic converters.

Xianyong Xiao received the B.S., M.S., and Ph.D. degrees from Sichuan University, Chengdu, China, in 1990, 1998, and 2010, respectively. He is currently a Professor in the College of Electrical Engineering, Sichuan University. His research interests include power quality, smart distribution system, power system catastrophic event, uncertainty theory and uncertain measure applied to power systems.

Shu Zhang received the B.S., M.S., and Ph.D. degrees in electrical engineering from Southwest Jiaotong University, Chengdu, China, in 2010, 2013, and 2018, respectively. Currently, she is a Research Assistant in the College of Electrical Engineering, Sichuan University, Chengdu, China. Her research interests include fault diagnosis and automation of distribution network, load analysis, and modelling by power disturbance data.

Jiandong Si received the B.S. degree in electrical engineering from Northeast Electric Power University, Jilin, China, in 1999, and the M.S. degree in electrical engineering from North China Electric Power University, Beijing, China, in 2011. He is currently an Engineer with the Taizhou Power Supply Company, State Grid Zhejiang Electric Power Company Limited, Taizhou, China. His main research interests include power quality control in microgrids and grid-connected control of renewable energy.